



Investigating the origin of exchange bias effect in ferromagnetic FeNi nanoparticles prepared via controlled synthesis

Kavita Kumari¹ · Akshay Kumar² · Ji Eun Lee¹ · Bon Heun Koo^{1,2}

Received: 9 March 2021 / Accepted: 4 May 2021 / Published online: 3 June 2021
© King Abdulaziz City for Science and Technology 2021

Abstract

In the present work, the FeNi nanoparticles have been synthesized using NaBH_4 reduced co-precipitation technique followed by annealing at 210 °C for 4 h in a simple box furnace. The nanoparticles were characterized using X-ray diffraction (XRD), Field emission scanning electron microscopy (FE-SEM), Energy-dispersive X-ray spectroscopy (EDS), Raman spectroscopy, and dc magnetization. The XRD analysis revealed the formation of dual phases (FeNi_3 ; FeNi) with face-centred cubic symmetry along with the additional phases of oxonium Ni oxide (NiOOH), hexagonal-Fe and iron peroxide (FeOOH). The FE-SEM micrographs demonstrated the evolution of dumb-bell shape morphology due to the heterogeneous growth of the nuclei resulting into agglomeration of particles. The XRD and FE-SEM collectively confirmed the nanometre (nm) dimensions of the particles. The mapping performed using EDS spectra validates the elemental compositions of the Nanoparticles. The Raman spectra reiterated the presence of impurity phases in addition to the trivial amount of NiO. The M–H (field dependent magnetization) hysteresis curves, plotted under the conditions of field cooled (FC) and zero field cooled (ZFC), shifted horizontally by $\sim 14\text{Oe}$ indicating presence of exchange bias. Alongside, FC-ZFC MT (temperature-dependent magnetization) curves also showed bifurcation at temperatures below 300 K that is also an indicative to the exchange bias. In brief, the exchange bias has been confirmed in ferromagnetic FeNi nanoparticles and the origin may be attributed to the exchange interactions at the particle interfaces having canted spins which emerge due to the presence of impurities and dual phases of FeNi.

Keywords Exchange bias · Spin canting · Hysteresis shift · Ferromagnetic · Heterogeneous nucleation

Introduction

Due to the magnetic anisotropy, the magnetic coupling between the canted spins at the interface of the particles results into a well-known phenomenon called exchange bias (EB) effect. The presence of uncompensated/canted spins or reorientation of spins, originated due to various factors like FM (ferromagnetic)–AFM (antiferromagnetic) interactions, defects, or impurities, etc. gives rise to the magnetic anisotropy in the material. This means that the energy required to

magnetize the material no longer remain same but varies for different directions of magnetization. The investigation of EB in functional materials has emerged as a distinguished issue in the second half of the previous century. Since its discovery in 1956, it has been greatly utilized in the fabrication of devices like magnetic recording discs, spin valves, etc., and has dramatically changed the technology by improving the information processing and magnetic data storage in the memory-based devices (Manchon and Zhang 2009; Wang et al. 2011). The EB effect has been observed in metal oxides, magnetic core–shell nanostructures, and intermetallic compounds. However, the materials like binary, ternary, and Heusler alloys such as Ni–Mn, Cu–Mn–Al, Ni_2MnGa , etc., that have been explored by far, exhibit operational EB at a temperature as low as 1.8 K or 5 K. The momentous value of H_{EB} reported is ~ 1300 Oe at 10 K in Ni–Mn–In bulk alloys (Giri et al. 2011; Wang et al. 2011). Likewise, in Ni–Mn–Sn, the $H_{\text{EB}} \sim 2500$ Oe at 10 K is reported which almost disappears when the temperature reaches to 70 K

✉ Bon Heun Koo
bhkoo@changwon.ac.kr

¹ Department of Material Science and Engineering, Changwon National University, Changwon, Gyeongnam 51140, Republic of Korea

² Department of Materials Convergence and System Engineering, Changwon National University, Changwon, Gyeongnam 51140, Republic of Korea

(Çakir et al. 2016). Worth noticing is that the existing reports in the published literature are primarily based on those alloy compounds which consider Mn, being an antiferromagnetic element, as an essential constituent; even so, the reported literature lacks the exploration and discussion on the EB effect in pure alloy nanoparticles.

Furthermore, the manifestation of EB is measured in terms of exchange bias field (H_{EB}) and can be identified by analysing the M–H hysteresis loop measured below a critical temperature known as blocking temperature. The change in the shape of the hysteresis like rotation or horizontal/vertical shift is a direct indication of the presence of the EB in the system; the genesis of which is fundamentally considered to lie in the systems containing FM/AFM interfaces and boundaries. However, besides FM/AFM systems, the EB effect has also been observed in ferrimagnetic/ferromagnetic and ferrimagnetic/ferrimagnetic systems (Manna and Yusuf 2014). Even the coupling interactions in amorphous alloy heterostructures, for instance [Pt/Co]₅₀/TbFe bilayers, have been found to originate the strong magnetic anisotropy (Schubert et al. 2013). Since the EB has also been detected in the systems exclusive of AFM interfaces, therefore, the shift in the hysteresis loop in such systems may be considered to be influenced by the dopants, impurities/defects, disorders, or presence of more than one phases (Vallejo-Fernandez et al. 2011; Preller et al. 2020). The impurities can possibly create canted spins in the system prompted by thermal agitations and provide the effective sites for the pinned spins. Fernandez et al. have proposed a domain wall pinning model which suggests that the increased concentration of the impurity transforms the multi-domain antiferromagnetic grain to the single-domain antiferromagnetic grain along with the reduction in the grain size. Above a particular grain diameter, the thermal instability creates a metastable state in the grain which increases the exchange bias in the system (Vallejo-Fernandez et al. 2011). This disclosure displays the role of the impurities to the enhancement of the EB. If a non-equilibrium develops a metastable state in a complete ferromagnetic system, then this may bring about the necessary exchange interactions and/or the spin–orbit interactions. This can enhance the magnetic anisotropy of the system leading to the desirable EB effect. In this manner, the impurity states present in the system may give rise to the spin–orbit interactions provided that the interactions are of inversion-symmetry broken type. Such interactions are likely to create the non-equilibrium spin density which couples to the local magnetization through ferromagnetic exchange interactions resulting into the rotation of magnetization, thus, induce a spin torque which accordingly may produce the EB effect. Manchon et al. have reported that the presence of impurity produces spin torque in a ferromagnetic single layer resulting into anisotropy (Manchon and Zhang 2009). In the same way, the presence of multiphases in a

system also provides the supportive conditions for the magnetic exchange interactions. For instance, the co-existence of two pure and ordered phases: fct FePt and fcc FePt₃, has been reported to generate a significant amount of EB field (387 Oe) at 5 K. The heat treatment of FePt above 500 °C results into the formation of two phases, i.e., fct FePt and fcc FePt₃ along with the elongation of the particles shaping like a dumb-bell. The interface boundaries of these phases become the origin of the magnetic exchange interactions (Preller et al. 2020). Thus, the presence of impurities and/or multiple phases in a ferromagnetic system are very likely to induce the magnetic anisotropy required to produce the EB effect.

Here, in this work, we have synthesized NaBH₄ reduced FeNi nanoparticles using co-precipitation technique and examined for the origin of EB effect. The nanoparticles were characterized through XRD, FE-SEM, Raman spectroscopy, and magnetization techniques. The investigations established the presence of weak EB at 50 K temperature that may be attributed to the impurities and dual phases of FeNi nanoparticles.

Materials and methods

Synthesis

FeNi nanoparticles were synthesized in the ratio 1:1, using co-precipitation method via reduction by means of NaBH₄. All the chemicals were purchased from Sigma-Aldrich and utilized as brought with 99.99% purity. To obtain the desired product, following two solutions were prepared simultaneously:

Solution I

The FeCl₃·6H₂O (270.30 g/mol) and NiCl₂·6H₂O (237.69 g/mol) were used as initial precursors. The stoichiometric amount of the precursors, in ratio 1:1, was taken in a beaker to make a solution of 0.015 M in 200 ml DI water. The solution was kept for stirring at 700 rpm for homogeneous dissolution of ions in the solvent at room temperature. After 30 min, the temperature was raised to 80 °C and maintained with stirring for 1 h. After 1 h the temperature was elevated to 100 °C and stirred for another 30 min.

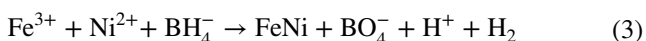
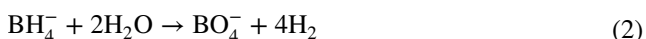
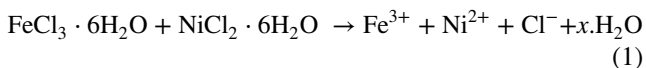
Solution II

The second solution was prepared by dissolving NaBH₄ in DI water. NaBH₄ was measured by keeping the molar ratio of metal to NaBH₄ as 1: 100. The solution was stirred at 700 rpm to mix homogeneously.

After the uniform mixing of salts, Solution II was added dropwise in Solution I to reduce the Fe^{3+} , Ni^{2+} ions to FeNi nanoparticles and form FeNi colloids. The reaction time was kept 10 min. As the NaBH_4 solution was added in Solution I, the solution turned from whitish to black. Once the whole solution II is dropped to solution I, the black precipitates could be seen very clearly. The precipitates were separated through centrifugation with subsequent washing using DI water and ethanol. The precipitates were dried overnight in a hot air oven at 80 °C. Afterwards, the obtained product was grinded and annealed at 210 °C for 4 h in a simple box furnace.

Chemical reactions involved

NaBH_4 is a very strong reducing agent utilized effectively for the generation of metallic nanoparticles. However, the composition of the final product is highly influenced by various factors like metal to NaBH_4 ratio, the preparation conditions such as rate and time of reaction or the thermal treatment, etc. The reaction of metal salts with NaBH_4 takes place in several steps described as below (Glavee et al. 1992; Shen et al. 1993; Shin et al. 2007; Mirzaei et al. 2017):



Dissolution of metal ions and hydrolysis of NaBH_4 are independent steps. When NaBH_4 solution is added to the metal salt solution gradually dropwise, the reaction takes

place very rapidly bringing about the formation of black-colored particulates within the nm size range. The BH_4^- ions reduce to BO_4^- by the aid of metal ions as catalysts. Thus, metals salts can be effectively reduced to the metal particles using BH_4^- . The reaction time was kept 10 min, because if the reaction time is increased, then the aging of NaBH_4 in the solution makes the colloid unstable which further may give rise to the formation of NaOH resulting into the agglomeration of the particles greater than nm range. Eventually, the formation of ultrafine particles is highly affected by the reaction conditions.

Mechanism

The solution saturates due to the dissolution of the ions (Fe^{3+} , Ni^{2+} , Cl^- , BH_4^-) followed by the formation of dual phases: FeNi_3 and FeNi . These two phases form phase boundaries having low surface energy. In addition to the primary phases, the rejected solute forms the impurities such as NiOOH , hexagonal-Fe, and FeOOH . The impurities move towards the phase boundaries of dual phases owing to the low energy of these boundaries and get accumulated. The presence of these boundaries further reduces the interfacial energy and provide heterogeneous sites by creating the spots of commotion for initiating the heterogeneous nucleation process. The heterogeneous nucleation becomes feasible, because at the interfaces, the free energy barrier reduces due to the low surface energy of the interface (Hong et al. 1993; Lu et al. 2006; Anumol et al. 2011; Smallman and Ngan 2013; Jana 2015; Chen et al. 2019). This heterogeneous nucleation, further, leads to the growth of large agglomerates. The mechanism of heterogeneous nucleation and growth of the dumb-bell shaped nanoparticles has been demonstrated using schematic in Fig. 1.

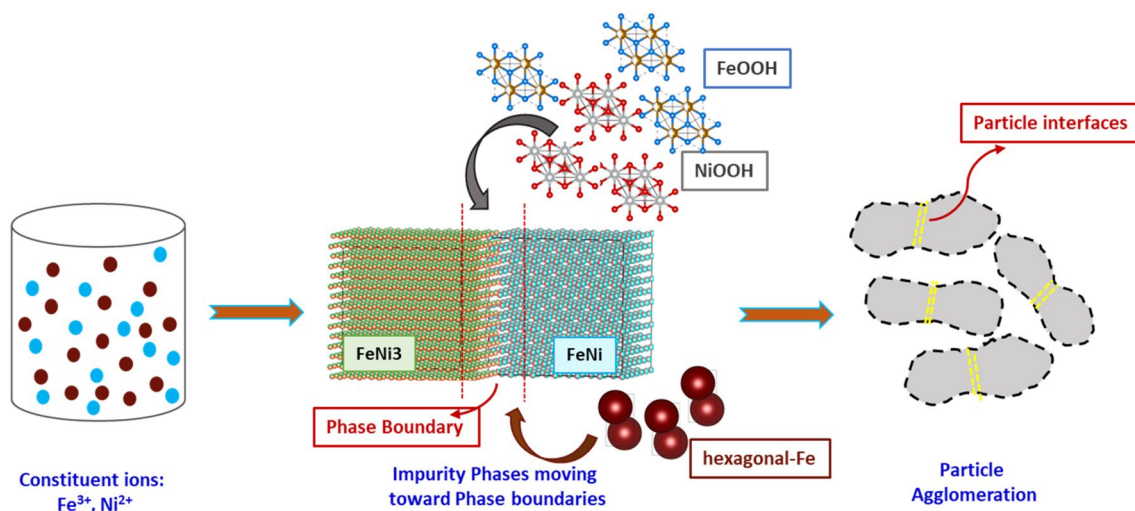


Fig. 1 Schematic demonstrating heterogeneous nucleation at the phase boundaries

Characterization

The resultant product was characterized using various characterization techniques, viz., XRD, FE-SEM, Raman spectroscopy, and Magnetization. The XRD patterns were obtained at PANalytical X'pert pro X-ray diffractometer ($\lambda_{\text{Cu-K}\alpha} = 0.154 \text{ nm}$) in the range $20^\circ \leq 2\theta \leq 80^\circ$ (step size = 0.016715). FE-SEM micrographs and EDS maps were scanned at Merlin compact at 5 kV and 15 kV, respectively. The Raman spectra were obtained at JASCO NRS-3300 Laser Raman Spectrometer at room temperature. The magnetization measurements were carried at VSM module of the cryogen-free physical property measurement system (PPMS), VersaLab developed by Quantum Design.

Results and discussion

XRD analysis

Figure 2a shows the XRD patterns of FeNi nanoparticles synthesized with 1:1 ratio. The patterns display the characteristic peaks of two main phases, i.e., FeNi₃ and FeNi; both possessing face-centred cubic (FCC) crystallinity with Fm-3 m space group along with impurity phases of hexagonal-Fe, NiOOH, and FeOOH (Hong and Fultz 1996). The peaks observed at 43.6°, 50.7°, and 74.7° reflect the (111), (200) and (220) planes of FeNi₃ phase corresponding to JCPDS number 47-1417 and the peaks lying adjacent to these peaks as their shoulder peaks correspond to the FeNi phase (Wu et al. 2010). The phase fraction has been calculated using the area under the curve. The FeNi₃ phase constitutes 48%, and the FeNi phase constitutes 30% of the total crystallinity as displayed in Fig. 2a, whereas, the remaining 22% is constituted by the impurity phases, i.e., hexagonal-Fe, NiOOH, and FeOOH. Since, elemental Ni possesses FCC structure, that means Fe might be substituted in Ni matrix for the formation of Fm-3 m phases. The enlarged view of (111) plane demonstrating distinct phases is displayed in Fig. 2b. The area shaded in yellow corresponds to FeNi₃ phase constituting 48% and the area shaded in pink corresponds to the FeNi phase constituting 30%. The phase formation has also been confirmed via Rietveld refinement of the XRD patterns, as shown in Fig. 2c. The black circles reflect the observed spectra, while the overlying red line corresponds to the theoretical calculated patterns with a difference as indicated by the purple line at the bottom. The vertical blue lines represent the Bragg's reflection. The refinement shows the formation of two phases corresponding to FeNi₃ and FeNi. The average crystallite size, as calculated using Scherrer's formula, has been found to be ~21 nm and the lattice parameters have been found to be 3.64 and 3.68 Å for FeNi₃ and FeNi phases, respectively (Soni et al. 2018).

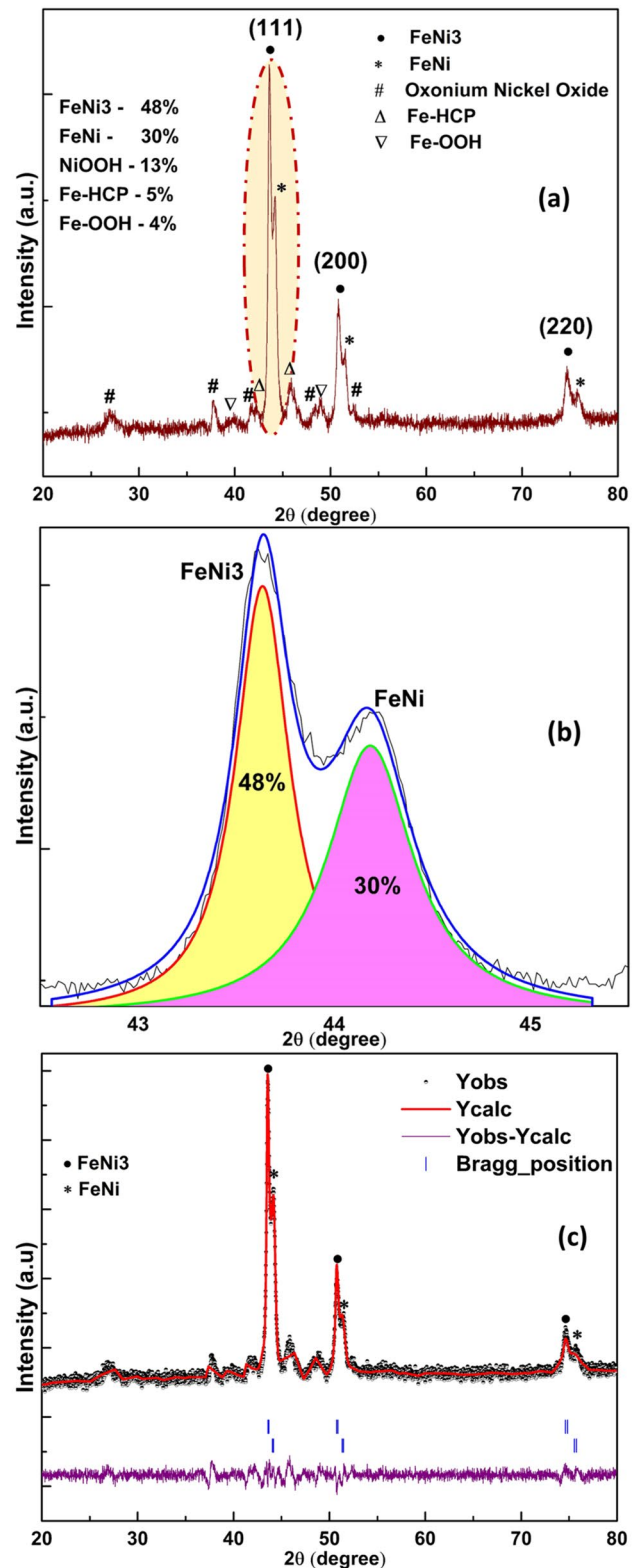


Fig. 2 a XRD spectra of FeNi nanoparticles; b Enlarged view of (111) peak; c Rietveld refinement of XRD patterns of FeNi nanoparticles

These values are in conformity with the existing literature (Wu et al. 2010). The reason of co-existence of parent and impurity phases along with the amalgamation of particles may dwell in the heterogeneous nucleation and conditions of the post-heat treatment of the particles (Koh et al. 2007). The process of annealing was carried in air atmosphere instead of any reducing environment. The annealing was carried at a temperature of 210 °C which explains the formation of NiOOH and FeOOH, because this temperature lies intermediate to the Neel temperature of NiO and FeO. Furthermore, at 210 °C, the possibility of NiO and FeO phase formation cannot be declined; however, no significant peak in the XRD spectra could be observed related to these phases. This reveals that the reduction of precursor salts carried under controlled addition of NaBH₄ might not require any gaseous/reducing environment during heat treatment. Nevertheless, stable single-phase formation of FeNi is quite challenging. Li et al. have reported the transformation between various phases of FeNi ultrafine nanoparticles with diameter less than 35 nm at different compositions of Fe and Ni (Li et al. 1997). However, in the present work, two phases of FeNi coexist together. The presence of dual phases indicates that the composition of Fe and Ni content has certainly changed in the final product which may depend on the difference of their physical properties like difference in vapour pressure of Fe and Ni, etc. (Li et al. 1997).

FE-SEM analysis

The FE-SEM image of FeNi nanoparticles is presented in Fig. 3a. The formation of dumb-bell shaped structures ranging from 40 to 90 nm is observed to be evolved from the spherical-shape morphology of the particles, as shown in inset of Fig. 3a. These dimensions are different than that obtained via Scherrer's formula because of the different techniques of measurement employed. The Scherrer's formula gives the crystallite dimensions, while the FE-SEM micrographs provide that of particle sizes. Furthermore, the evolution of large agglomerates may have been resulted from the amalgamation of the nuclei during the growth. Due to this, the particles attain a low energy state by undergoing reduction at the particle interfaces, withal, the morphological dimensions remain in nm range (Panta and Bergmann 2015). Such type of agglomeration and inhomogeneous grain size in FeNi nanoparticles has previously been reported by Santos et al. (Dos Santos et al. 2016). The amalgamation of the particles is considered to create interface boundaries which give rise to the canted spins as shown in enlarged view of a particle in Fig. 3a. The confined dimensions also contribute to the canting of spins. Li et al. have discussed that when the particle dimensions are reduced to nano-size, the spins at the surface of the particle do not get completely aligned along the applied magnetic field, but make a canting angle with the

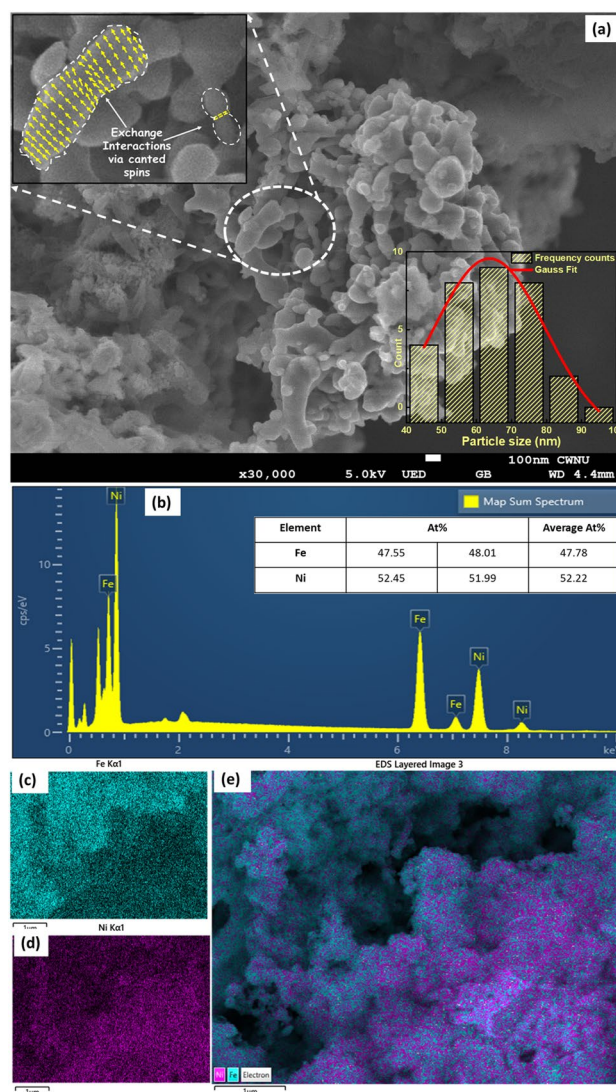


Fig. 3 a FE-SEM micrographs of FeNi nanoparticles; inset demonstrates canted spins in the dumb-bell shaped particles; b-e EDS spectrum and mapping of FeNi Nanoparticles

field (Li et al. 1997). Moreover, to analyse the microstructure quantitatively, the energy-dispersive X-ray spectra of FeNi nanoparticles have been investigated as displayed in Fig. 3b, which confirm the presence of these elements in the Nanoparticles. It can be observed that Ni compose of about 52% and Fe compose of about 48% of the total phases, as shown in inset of Fig. 3b. The elemental mapping of individual Ni, Fe is shown in Fig. 3c, d, respectively. The layered image containing both the elements (Fig. 3e) reveals that a region of the map illustrates more Ni content that validates the formation of two phases, i.e., FeNi and FeNi₃ as obtained by XRD analysis.

Furthermore, the size distribution of the particles depends on the nucleation process during growth. The uniform size nanoparticles can be obtained if the nucleation is

homogeneous. However, the non-uniform particle size and the formation of large agglomerates may be associated with the heterogeneous nucleation process (Jana 2015).

Raman analysis

The presence of impurities has been investigated via Raman spectroscopy by utilizing the molecular disorders arising due to the lattice vibrations. These vibrations result from the interaction of the molecules with the irradiated energy and can be recorded as broad peaks known as Raman spectra, however, it is noteworthy that the characteristic peaks may be influenced by the power of the laser source. The obtained spectra give a great deal of information about the nature of species and molecular disorders present in the material (Panta and Bergmann 2015). The Raman spectra of FeNi nanoparticles are demonstrated in Fig. 4. The spectral features are discernible at 364, 540, 756, 860, and 1085 cm^{-1} . The trivial band at low frequency of 364 cm^{-1} is attributable to the E_{2g} active mode of hexagonal-Fe. The α and γ phases of Fe do not exhibit first-order Raman response (Merkel et al. 2000). Another striking feature appearing at 540 cm^{-1} may be assigned to the Ni–O vibrational unit (Zhang et al. 2021). This is peculiar, because no peaks corresponding to NiO could be observed in XRD patterns. Next, two bands appearing at 756 and 860 cm^{-1} belong to the complexes of FeOOH (iron peroxide) attributable to the active (O–O) vibrational unit (Ho et al. 1999). These bands indicate the charge transfer between the peroxide to Fe. Furthermore, a broad peak appearing at 1082 cm^{-1} corresponds to the stretching modes (O–O) of active oxygen in NiOOH vibrations. It is apparent from previous reports that the formation of alloy nanoparticles is usually accompanied with the oxides and hydroxides of the metals. As an instance, Cole

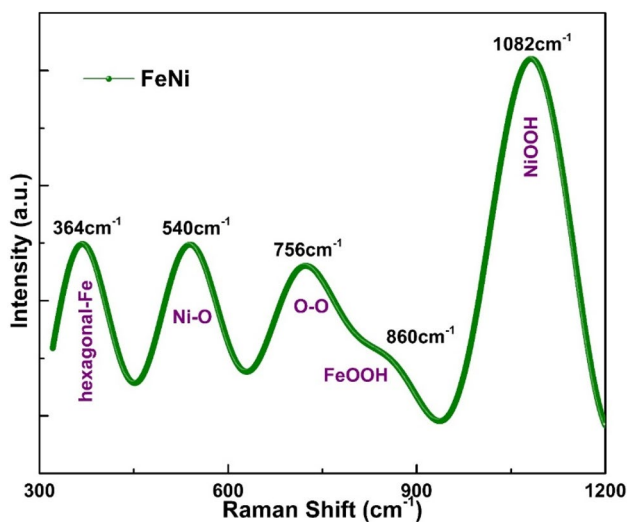


Fig. 4 Raman spectra of FeNi nanoparticles

et al. have reported that in amorphous alloys, the metal oxide formation is more prominent, while in crystalline alloys, the metal hydroxides are preferentially formed (Diaz-Morales et al. 2016; Cole et al. 2018).

Magnetization

The M–H curves of FeNi nanoparticles at 300 K and 50 K temperature are displayed in Fig. 5a. The magnetization curves at 50 K are measured under the conditions of FC and ZFC. All the curves exhibit small hysteresis indicating weak ferromagnetic behaviour. The magnetization shows saturation at 30 kOe with enhancement in all the parameters while reducing the temperature from 300 to 50 K as presented in Table 1. The saturation magnetization (M_s) increases from 83 to 96 emu/g along with the enhancement in the remnant

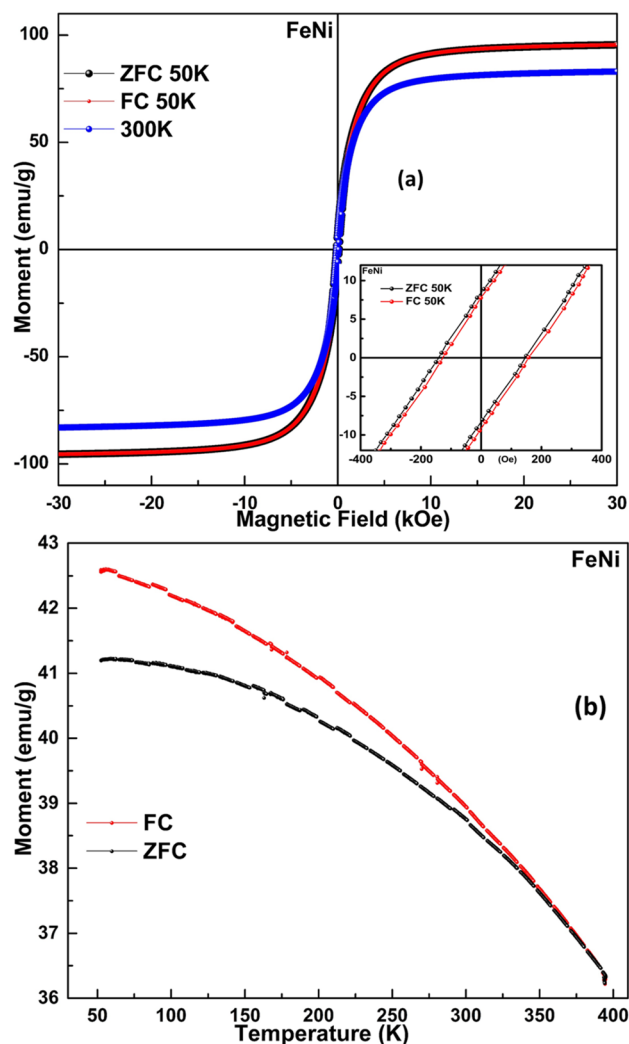
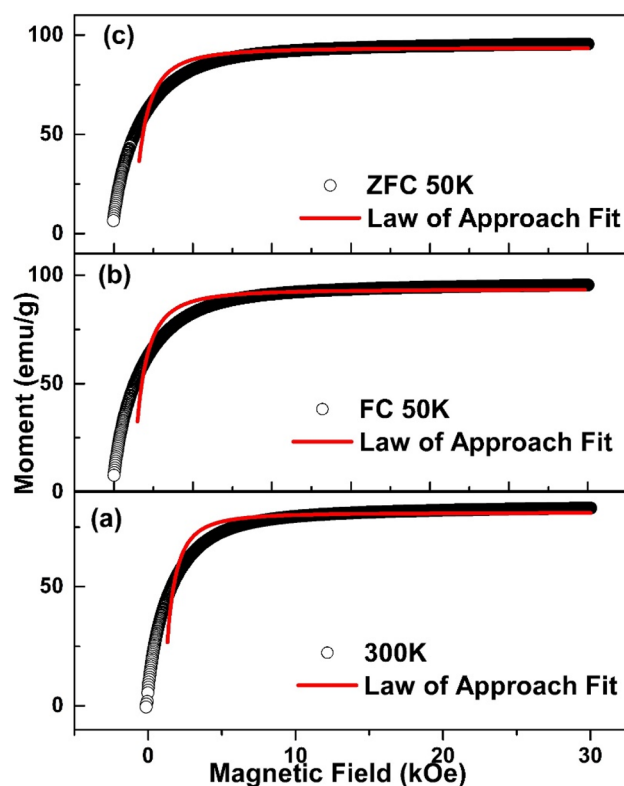


Fig. 5 **a** M–H hysteresis curves at ± 30 kOe; inset shows the hysteresis in the range ± 400 Oe and **b** MT curve under FC and ZFC conditions

Table 1 The magnetization parameters obtained from M–H hysteresis curves of FeNi nanoparticles

Magnetization condition	M_s (emu/g)	M_r (emu/g)	H_c (Oe)	K ($\times 10^4$ erg/cm ³)
300 K	83	7.2	121	3.9
50 K-FC	96	7.8	127	5.2
50 K-ZFC	96	8.4	141	5.4

magnetization (M_r) from 7.2 emu/g to 8.4 emu/g and coercivity (H_c) from 121 to 141 Oe. However, M_s remains invariant at 50 K under both the cooling conditions, though with increasing coercivity from 127 to 141 Oe. Furthermore, the effect of FC and ZFC at 50 K can be observed through the shift in hysteresis along x -axis as shown in inset of Fig. 5a. The hysteresis shifts ~ 14 Oe towards the right which gives the measure of the exchange bias magnetic field (H_{EB}). Although the value of H_{EB} observed in the present case is very small, however, is very encouraging, because the exchange bias obtained thus far in metallic nanoparticles is at very low temperatures (~ 5 K) (Giri et al. 2011; Preller et al. 2020). The exchange bias field of ~ 14 Oe at 50 K may be attributed to the canted spins in the sample that arise at the particle interfaces due to the different spin states on both sides of the particle interfaces. The enhancement in the coercivity under FC condition may be explained using spin glass model as described by Zaineb Hussain et al. for FM/AFM layers. Since the present system does not contain AFM elements, therefore a low anisotropy region may be created at the interfaces which may enhance the coercivity (Nogués and Schuller 1999; Hussain et al. 2017). P. K. Manna et al. have discussed a strong interface exchange coupling amongst two ferromagnetic components (Manna and Yusuf 2014). In addition to the hysteresis shift, the presence of exchange bias can also be established from the FC-ZFC MT plots as displayed in Fig. 5b. The bifurcation in FC-ZFC MT curves starts below ~ 300 K and increases as the temperature reduces to 50 K. This bifurcation at 50 K temperature also points towards the occurrence of exchange interactions between the canted spins. The origin of exchange bias in this system relies upon the heterogeneous nucleation carried growth of the particles followed by heat treatment which results into large dumb-bell shaped agglomerates as observed from the FE-SEM micrographs. These agglomerates establish canted spins at the particle interfaces. The canted spins alter the spin structure on the two sides of the interface. Due to different spin structure, the spins undergo exchange interactions and the eventual exchange coupling between the spins gives rise to the exchange anisotropy resulting into a metastable state which further directs the magnetic behaviour of the material (Vasilakaki and Trohidou 2009). There could be various possible reasons for the

**Fig. 6** The law of approach fit of FeNi nanoparticles at **a** 300 K, **b** 50 K-FC, and **c** 50 K-ZFC

formation of the metastable state as discussed by Anirudha Ghosh et al. (Ghosh et al. 2015). Basically, a metastable state is formed when the system has sufficiently high anisotropy which can reserve the necessary magnetic energy barrier to hinder the thermal switching of the moments. Balan et al. have reported the presence of metastable ferromagnetic state in structurally excited Fe nanoparticles in which a ferromagnetic and superparamagnetic state coexist together (Balan et al. 2014). Thereby, the existence of the metastable state prompt the required exchange coupling. Additionally, the magnetic anisotropy constant has been calculated using the law of approach (Kumar et al. 2013). The law of approach fit of FeNi nanoparticles at 300 K, 50 K-FC, and 50 K-ZFC conditions is displayed in Fig. 6. The values of anisotropy constants are indicated in Table 1. It can be observed that the value of anisotropy constant increases when temperature is reduced to 50 K. However, there is no significant difference due to FC and ZFC conditions.

Moreover, when the bimetallic interfaces are formed, they are much likely to induce defects and disorders in their vicinity which disturbs the symmetry of the system (Yaniv 1980). Although for such exchange coupling, conventionally, the interface boundary is expected to be of FM/AFM nature, however, the canted spins at the interfaces are also possible for systems like the present one including

ferromagnetic–ferromagnetic phases as discussed above. There are ample reports published on the exchange interactions in the ferromagnetic systems, mainly constituting of transition metals having unpaired *d*-electrons (Manchon and Zhang 2009; Ghosh et al. 2015; Kanhe et al. 2016). Therefore, it is suggestive that the EB arising in the FeNi nanoparticles possessed with the impurities and dual phases may be attributed to the canted spins at the particle interfaces.

Conclusion

In summary, the FeNi nanoparticles were successfully prepared through controlled experimental conditions. The nanoparticles were characterized using XRD, FE-SEM, EDS, Raman spectroscopy, and dc magnetization. The XRD analysis revealed the formation FeNi₃ and FeNi phases having face-centred cubic crystallinity with Fm-3 m space group along with the impurity phases of NiOOH, hexagonal-Fe, and FeOOH. As estimated by Scherrer's equation, the crystallite size was found to be ~21 nm along with the lattice parameter of 3.64 and 3.68 Å for both the phases. The dumbbell shape morphology of the particles, demonstrated in the FE-SEM micrographs, may be originated due to the heterogeneous growth of the nuclei. Such growth agglomerated the particles during the synthesis as well as post-heat treatment resulting into the formation of interface boundaries between the particles. The elemental mapping via EDS confirmed the compositions of Fe and Ni. The Raman spectra confirms the impurity phases as revealed by XRD analysis in addition to the trivial NiO phase. The magnetization analysis performed under different conditions of temperature and magnetic field provided key evidence for the exchange bias in the present system. The hysteresis curves demonstrated ferromagnetic behaviour with increasing Ms (83 emu/g to 96 emu/g) and Hc (121–141 Oe) through the reduction of temperature from 300 to 50 K. The FC-ZFC M–H curves exhibited horizontal shifting by ~14 Oe at 50 K indicating presence of exchange bias. Moreover, FC-ZFC MT curves also demonstrated bifurcation at temperature below 300 K which increases with reducing temperature. Consequently, the origin of exchange bias in ferromagnetic FeNi nanoparticle may be attributed to the exchange interactions taking place between the canted spins at the particle interfaces.

Acknowledgements Support for this project comes from the National Research Foundation of Korea Grant funded by the Korean government (No. 2018R1D1A1B07046937). Support for this project also comes from the National Research Foundation of Korea Grant funded by the Korean government (No. 2020R111A3073553).

Declarations

Conflict of interest The authors have no conflict of interest.

References

- Anumol EA, Kundu P, Deshpande PA et al (2011) New insights into selective heterogeneous nucleation of metal nanoparticles on oxides by microwave-assisted reduction: rapid synthesis of high-activity supported catalysts. *ACS Nano* 5:8049–8061. <https://doi.org/10.1021/nn202639f>
- Balan A, Derlet PM, Rodríguez AF et al (2014) Direct observation of magnetic metastability in individual iron nanoparticles. *Phys Rev Lett* 112:107201. <https://doi.org/10.1103/PhysRevLett.112.107201>
- Çakir A, Acet M, Farle M (2016) Exchange bias caused by field-induced spin reconfiguration in Ni-Mn-Sn. *Phys Rev B* 93:094411. <https://doi.org/10.1103/PhysRevB.93.094411>
- Chen PC, Liu M, Du JS et al (2019) Interface and heterostructure design in polyelemental nanoparticles. *Science* 363:959–964
- Cole KM, Kirk DW, Thorpe SJ (2018) In Situ Raman study of amorphous and crystalline Ni-Co alloys for the alkaline oxygen evolution reaction. *J Electrochem Soc* 165:J3122–J3129. <https://doi.org/10.1149/2.0131815jes>
- Diaz-Morales O, Ferrus-Suspedra D, Koper MTM (2016) The importance of nickel oxyhydroxide deprotonation on its activity towards electrochemical water oxidation. *Chem Sci* 7:2639–2645. <https://doi.org/10.1039/c5sc04486c>
- Dos Santos CM, Martins AFN, Costa BC et al (2016) Synthesis of FeNi alloy nanomaterials by proteic Sol-Gel method: crystallographic, morphological, and magnetic properties. *J Nanomater* 2016:9. <https://doi.org/10.1155/2016/1637091>
- Ghosh A, Paul S, Raj S (2015) Understanding bifurcations in FC-ZFC magnetization of dilutely Fe³⁺ doped CdS nanoparticles. *Solid State Commun* 208:1–6. <https://doi.org/10.1016/j.ssc.2015.02.010>
- Giri S, Patra M, Majumdar S (2011) Exchange bias effect in alloys and compounds. *J Phys Condens Matter* 23:073201. <https://doi.org/10.1088/0953-8984/23/7/073201>
- Glavee GN, Klabunde KJ, Sorensen CM, Hadjapanayis GC (1992) Borohydride reductions of metal ions. a new understanding of the chemistry leading to nanoscale particles of metals, borides, and metal borates. *Langmuir* 8:771–773. <https://doi.org/10.1021/la00039a008>
- Ho RYN, Roelfs G, Feringa BL, Que L (1999) Raman evidence for a weakened O-O bond in mononuclear low-spin iron(III)-hydroperoxides. *J Am Chem Soc* 121:264–265. <https://doi.org/10.1021/ja982812p>
- Hong LB, Fultz B (1996) Two-phase coexistence in Fe-Ni alloys synthesized by ball milling. *J Appl Phys* 79:3946–3955. <https://doi.org/10.1063/1.361821>
- Hong T, Smith JR, Srolovitz DJ (1993) Impurity effects on adhesion: Nb, C, O, B, and S at a Mo/MoSi₂ interface. *Phys Rev B* 47(13):615
- Hussain Z, Kumar D, Reddy VR, Gupta A (2017) Kerr microscopy study of exchange-coupled FePt/Fe exchange spring magnets. *J Magn Magn Mater* 430:78–84. <https://doi.org/10.1016/j.jmmm.2017.01.052>
- Jana S (2015) Advances in nanoscale alloys and intermetallics: low temperature solution chemistry synthesis and application in catalysis. *Dalt Trans* 44:18692–18717. <https://doi.org/10.1039/c5dt03699b>
- Kanhe NS, Kumar A, Yusuf SM et al (2016) Investigation of structural and magnetic properties of thermal plasma-synthesized Fe_{1-x}Ni_x alloy nanoparticles. *J Alloys Compd* 663:30–40. <https://doi.org/10.1016/j.jallcom.2015.11.190>
- Koh S, Yu C, Mani P et al (2007) Activity of ordered and disordered Pt-Co alloy phases for the electroreduction of oxygen in catalysts with multiple coexisting phases. *J Power Sources* 172:50–56. <https://doi.org/10.1016/j.jpowsour.2007.01.002>

- Kumar L, Kumar P, Kar M (2013) Cation distribution by Rietveld technique and magnetocrystalline anisotropy of Zn substituted nanocrystalline cobalt ferrite. *J Alloys Compd* 551:72–81. <https://doi.org/10.1016/j.jallcom.2012.10.009>
- Li XG, Chiba A, Takahashi S (1997) Preparation and magnetic properties of ultrafine particles of Fe-Ni alloys. *J Magn Magn Mater* 170:339–345
- Lu L, Dahle AK, StJohn DH (2006) Heterogeneous nucleation of Mg-Al alloys. *Scr Mater* 54:2197–2201. <https://doi.org/10.1016/j.scriptamat.2006.02.048>
- Manchon A, Zhang S (2009) Theory of spin torque due to spin-orbit coupling. *Phys Rev B* 79:094422. <https://doi.org/10.1103/PhysRevB.79.094422>
- Manna PK, Yusuf SM (2014) Two interface effects: exchange bias and magnetic proximity. *Phys Rep* 535:61–99. <https://doi.org/10.1016/j.physrep.2013.10.002>
- Merkel S, Goncharov AF, Mao HK et al (2000) Raman spectroscopy of iron to 152 gigapascals: implications for earth's inner core. *Science* 288:1626–1629
- Mirzaei A, Janghorban K, Hashemi B et al (2017) Characterization and optical studies of PVP-capped silver nanoparticles. *J Nanostructure Chem* 7:37–46. <https://doi.org/10.1007/s40097-016-0212-3>
- Nogués J, Schuller IK (1999) Exchange bias. *J Magn Magn Mater* 192:203–232. [https://doi.org/10.1016/S0304-8853\(98\)00266-2](https://doi.org/10.1016/S0304-8853(98)00266-2)
- Panta P, Bergmann C (2015) Raman spectroscopy of iron oxide of nanoparticles (Fe₃O₄). *J Mater Sci Eng* 5:4–6. <https://doi.org/10.4172/2169-0022.1000217>
- Preller T, Knickmeier S, Menzel D et al (2020) Exchange bias in FePt-FePt₃ thin films by controlled phase transition of blended nanoparticle building blocks. *Langmuir* 36:2093–2101. <https://doi.org/10.1021/acs.langmuir.9b02880>
- Schubert C, Hebler B, Schletter H et al (2013) Interfacial exchange coupling in Fe-Tb/[Co/Pt] heterostructures. *Phys Rev B* 87:054415. <https://doi.org/10.1103/PhysRevB.87.054415>
- Shen J, Li Z, Yan Q, Chen Y (1993) Reactions of bivalent metal ions with borohydride in aqueous solution for the preparation of ultrafine amorphous alloy particles. *J Phys Chem* 97:8504–8511. <https://doi.org/10.1021/j100134a020>
- Shin SJ, Kim YH, Kim CW et al (2007) Preparation of magnetic FeCo nanoparticles by coprecipitation route. *Curr Appl Phys* 7:404–408. <https://doi.org/10.1016/j.cap.2006.09.012>
- Smallman RE, Ngan AHW (2013) *Modern physical metallurgy*, 8th edn. Elsevier
- Soni S, Kumar S, Dalela B et al (2018) Defects and oxygen vacancies tailored structural and optical properties in CeO₂ nanoparticles doped with Sm³⁺ cation. *J Alloys Compd* 752:520–531. <https://doi.org/10.1016/j.jallcom.2018.04.157>
- Vallejo-Fernandez G, Kaeswurm B, O'Grady K (2011) Defect and impurity effects in exchange bias systems. *J Appl Phys* 109:07D738. <https://doi.org/10.1063/1.3556926>
- Vasilakaki M, Trohidou KN (2009) Numerical study of the exchange-bias effect in nanoparticles with ferromagnetic core/ferrimagnetic disordered shell morphology. *Phys Rev B* 79:144402. <https://doi.org/10.1103/PhysRevB.79.144402>
- Wang BM, Liu Y, Ren P et al (2011) Large exchange bias after zero-field cooling from an unmagnetized state. *Phys Rev Lett* 106:077203. <https://doi.org/10.1103/PhysRevLett.106.077203>
- Wu H, Qian C, Cao Y et al (2010) Synthesis and magnetic properties of size-controlled FeNi alloy nanoparticles attached on multiwalled carbon nanotubes. *J Phys Chem Solids* 71:290–295. <https://doi.org/10.1016/j.jpcs.2009.12.079>
- Yaniv A (1980) Theory of vacancies near a bimetallic interface. *Phys Rev B* 22:4776–4783. <https://doi.org/10.1103/PhysRevB.22.4776>
- Zhang G, Zeng J, Yin J et al (2021) Iron-facilitated surface reconstruction to in-situ generate nickel-iron oxyhydroxide on self-supported FeNi alloy fiber paper for efficient oxygen evolution reaction. *Appl Catal B Environ* 286:119902. <https://doi.org/10.1016/j.apcatb.2021.119902>

Publisher's Note Springer Nature remains neutral with regard to jurisdictional claims in published maps and institutional affiliations.